

Iranian Journal of Oil & Gas Science and Technology, Vol. 10 (2021), No. 3, pp. 49–68
<http://ijogst.put.ac.ir>

Evaluation of a Novel Mechanistic Approach to Predicting Transport of Water and Ions through Shale

Nima Hamidian Shoormasti¹ and Seyyed Alireza Tabatabaei-Nezhad^{2*}

¹ Ph.D. Candidate, Sahand Oil and Gas Research Institute, Faculty of Petroleum and Natural Gas Engineering, Sahand University of Technology, Tabriz, Iran

² Professor, Faculty of Petroleum and Natural Gas Engineering, Sahand Oil and Gas Research Institute Sahand University of Technology, Tabriz, Iran

Highlights

- The Revil model for ionic transport has been extended for multivalent ions.
- A simplified equation to estimate ion selectivity has been introduced.
- Correlation of ion selectivity with membrane efficiency has been proved.
- The model predicted the membrane efficiency data with a high correlation.

Received: April 14, 2021; revised: June 20, 2021; accepted: July 01, 2021

Shale formations are essential for different disciplines, including wellbore stability studies in petroleum engineering. In shale stability studies, the prediction of transport parameters of water and ions is a significant issue (Farrokhrouz and Asef, 2013). A unique and novel method to address this subject is the Revil model (Revil et al., 2011), which, unlike previous models, considers physiochemical mechanisms in the pore space and needs a few easily measurable shale properties (Revil et al., 2004). In this paper, for the first time to our knowledge, the Revil model has been extended for salts of multivalent ions. The extended model for water and ion transport through shale has been evaluated against a range of experimental data sets in the literature. The extended Revil model only needs a few shale properties such as cation exchange capacity (CEC), porosity, and grain density, which can be readily measured in the laboratory. Further, in the present work, three parameters ($f_Q, \beta_{(+)}^S, \nu$) have been considered calibration parameters. In addition to extending the Revil model for multivalent salts, we derived a simplified equation to estimate ion selectivity (IS) and a proof for the conjecture that IS correlates with membrane efficiency (ME). Focusing on the data set of Albazali (2005), a complete matching could be obtained by adjusting calibration parameters for each test data. In the case of adjusting all experiments with only three standard calibration parameters, the prediction was not satisfactory. However, the “intact-anion method” results were more accurate than the “Donnan method”. When multiple sets of ME data in a broader concentration range, including low concentrations, were plotted along with high-concentration data, correlativity was significant ($R^2 > 0.9$). Further, a sensitivity analysis of the model parameters was performed. Our findings pave the way for the appropriate mechanistic approach to investigating and handling practical engineering challenges associated with shale.


Keywords: Donnan method, Intact-anion method, Ion selectivity, Membrane efficiency, Updated Revil model

*Corresponding author:

Email: Tabatabaei@sut.ac.ir

How to cite this article

Hamidian Shoormasti N, Tabatabaei-Nezhad. S.A , *Evaluation of a Novel Mechanistic Approach to Predicting Transport of Water and Ions Through Shale*, Iran J. Oil Gas Sci. Technol., Vol. 10, No. 3, pp. 49–68, 2021.

DOI: <http://dx.doi.org/10.22050/ijogst.2021.136167>, This is an Open Access article under Creative Commons Attribution 4.0 International License. (creativecommons.org/licenses/by/4.0) 

1. Introduction

Shales are fine-grained sedimentary rocks with an average or high clay mineral content. The characteristic feature of shales is their foliation or breakage along the surface of layering (Farrokhrouz and Asef, 2013). Because of their unique behavior, these rocks cause many problems during drilling practice. Shales consist of more than 75% of all drilled formations, and more than 70% of well problems are related to shale instability (Lal, 1990). Water and ion movement into or out of the shale can change the stress state in the shale by altering the pore pressure. The penetration of water into the shale can also cause swelling and chemical weakening of the shale, leading to the collapse of the shale formation (Moslemizadeh and Shadizadeh, 2015). All these points and environmental problems associated with using non-water-based drilling fluids highlight the significance of predicting water and ion movement in shale.

On the other hand, the possibility of performing experiments such as pressure transmission test (PT test) is limited due to the difficulty of obtaining intact in-situ shale core plugs preserved under initial conditions (Chenevert et al., 2001) and performing the PT tests. Therefore modeling the ion and water transport gains further importance. The main transport properties of shales that have been considered in previous investigations are membrane efficiency, also called reflection coefficient, (Malusis et al., 2003), osmotic efficiency (Revil et al., 2004), or electro-osmotic coefficient (Malusis et al., 2003), diffusion coefficient (Revil et al., 2004; Malusis et al., 2003; Dominnijanni et al., 2017a,b), and ion selectivity (Albazali, 2005). Furthermore, transport modeling provides constitutive equations for transport fluxes in terms of gradients.

Some researchers proposed semi-empirical phenomenological models, such as the model introduced by Kedem and Kachalsky (1958), which is based on non-equilibrium thermodynamics. Nevertheless, these models did not explicitly consider the microstructural textural properties or electrical properties of the fluid-rock interface (Revil, 2011). Several mechanistic models have been proposed that consider the microstructure and electrical properties of the rock-fluid interface. A space-charge capillary model has been proposed by Gross and Osterle (1968) for charged porous media. They obtained formula to calculate the nine coefficients that couple different transport phenomena. Basu and Sharma (1997) modified the governing equations to consider the finite ion size, ion hydration, and dielectric constant variations later. Lomba et al. (2000) developed a space-charge model to simulate water and ion transport in shales. Hydraulic pressure, concentration, and electrical potential were considered deriving forces for water and solute flow between the two solutions separated by shale (Lomba et al., 2000). However, the above-mentioned analytical models are not readily applicable to the systematic experimental studies of petroleum engineering.

Spiegler et al. (1956) related the electrical conductivity to membrane potential for ion-exchange resins by introducing an analogy between pore fluid conductivity and a three-resistor circuit. However, their model did not account for the connection of macro and microscopic electrical transport processes, and the electrical double layer was not considered explicitly. Moreover, Sen (1989) indicated that their model is oversimplified because they did not consider the transport of both anions and cations.

The model introduced by Sen (1989) captured the effect of microgeometry of the porous media on membrane potential and electrical conductivity. He took into account different tortuosities for anions

and cations. Further, Revil et al. (2018) implemented the Padé approximant approach merely for predicting the electrical conductivity and not for modeling membrane transport processes.

However, Revil (1999) argued that the model of Sen (1989) had several drawbacks significantly akin to being used in practical applications: 1) the four independent parameters to describe the influence of microgeometry are very difficult to obtain by experiments (Revil, 1999); 2) Using Padé approximant to connect low and high salinity ranges is just an approximation. Therefore, Revil et al. (1999) introduced his model for membrane processes which was further developed in Revil et al. (2004), (2011), (2017a,b).

Revil et al. (2011) first upscaled the local transport equations, i.e., Stokes and Nernst-Planck, to the scale of a single capillary saturated with a 1:1 electrolyte. Then, these equations were upscaled to the scale of a network of capillaries embedded in a homogeneous and continuous mineral matrix.

The Revil model (2011) was only applicable for salts of monovalent ions (i.e., 1:1 salt such as NaCl); therefore, it should be extended for salts of multivalent ions (such as CaCl_2). This paper extended that model to obtain membrane efficiency and electrochemical potential across shale between two solutions with different concentrations of monovalent or multivalent salts. Then, the model outputs were compared with corresponding values obtained experimentally by Albazali (2005) and with multiple data sets from the literature.

This paper presented a novel analytical proof for the direct relation between ion selectivity and membrane efficiency. We also found a simple mechanistic formula for ion selectivity that appears unique. Moreover, we did not find any previous study on membrane efficiency or ion selectivity for salts of multivalent ions.

2. Theory

This section briefly explains the transport model by Revil et al. (2011) and our additional derivations. The nomenclature section shows a list of symbols and abbreviations used and their meanings and units. The ionic concentration in pore space is disturbed because of the negative charge of clay particles in shale. The Revil model assumes that instead of Poisson–Boltzmann distribution, ionic concentrations in the pore water is estimated either by the Donnan method (Revil et al., 2011) or by intact-anion method (Revil, 2015), and the system is considered locally in the equilibrium (thermodynamic) state. Further, the transport occurs only in micropores (Figure 1b), a fair assumption when working with shales (Revil, 2004).

The pore space is modeled as a set of unconnected capillaries with charged walls (Figure 1c and d). In general, the radius of capillaries has a distribution, but here, we assume a constant capillary radius for easiness. In the three-layer model (TLM) (Revil, 2004), it is assumed that the countercharge is divided between the Stern layer, which is adjacent to the rock-fluid interface and the diffuse layer (Figure 1c). f_Q denotes the ratio of countercharge in the Stern layer to the pore fluid charge.

It is assumed that the electrochemical potentials of cations and anions in the pore space and a fictitious reservoir in equilibrium with the pore space (Figure 1a) are equal to obtain the ionic concentrations in the pore space by the Donnan method. Ionic concentrations are obtained from Revil (2011) as follows.

$$\bar{C}_{(\pm)} = C_f (\sqrt{1 + \Theta^2} \pm \Theta) \quad (1)$$

The dimensionless parameter Θ is defined as:

$$\theta \equiv \frac{\bar{Q}_v^0}{2 e C_f} \quad (2)$$

where the effective charge per pore volume of the shale (\bar{Q}_v^0) is expressed by:

$$\bar{Q}_v^0 = \frac{\rho_g(1-\phi)(96320 \text{ CEC})(1-f_Q)}{\phi} \quad (3)$$

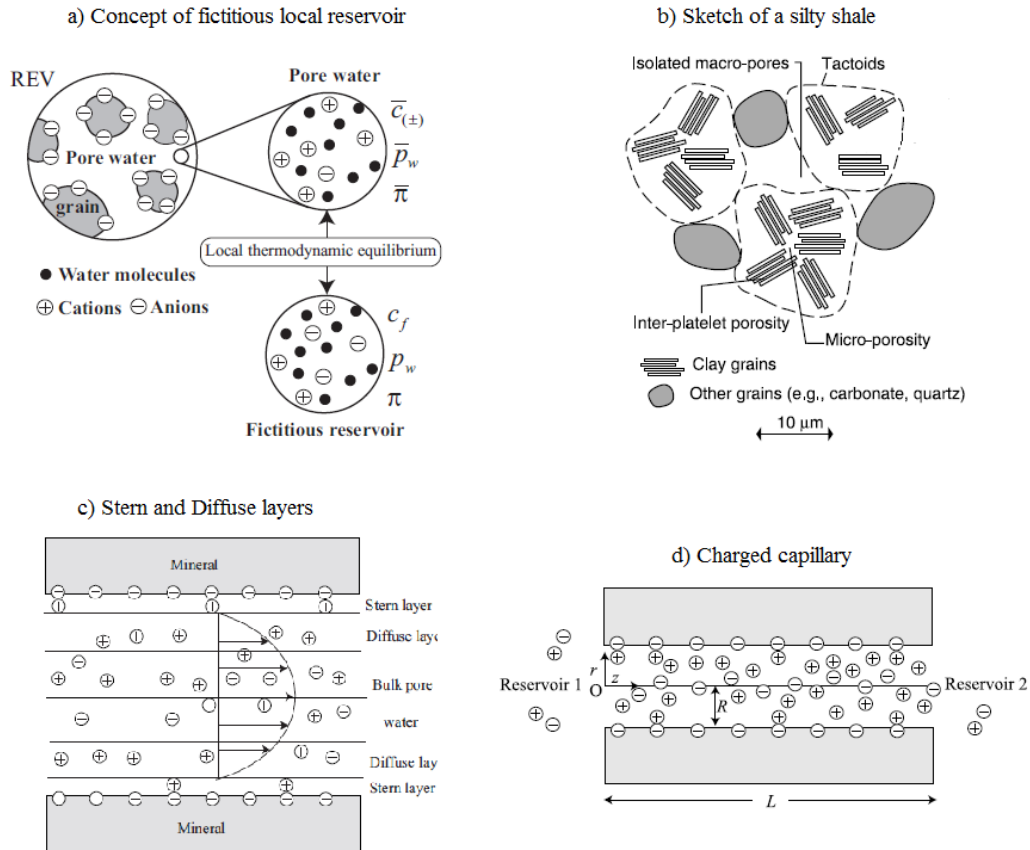


Figure 1

a) Concept of the fictitious local reservoir, b) sketch of a silty shale, c) Stern and diffuse layer in a capillary, and d) a charged capillary model for shale located between two reservoirs (Revil et al., 2004, 2011, and 2017).

We have generalized Equation (1), which is valid only for monovalent 1:1 salts, to a salt having several $v_{(+)}$ cations with charge $\omega_{(+)}$ and a number of $v_{(-)}$ anions with charge $\omega_{(-)}$ as follows (see Appendix A):

$$\frac{\omega_{(+)}}{\omega_{(-)}} \bar{C}_{(+)}^{\frac{\omega_{(-)}}{\omega_{(+)}}+1} - \left(\frac{\bar{Q}_v^0}{\omega_{(-)} e} \right) \bar{C}_{(+)}^{\frac{\omega_{(-)}}{\omega_{(+)}}} - \left(v_{(-)} v_{(+)} \frac{\omega_{(-)}}{\omega_{(+)}} C_f^{\frac{\omega_{(-)}}{\omega_{(+)}}+1} \right) = 0 \quad (4)$$

$$\bar{C}_{(-)} = \frac{\omega_{(+)}}{\omega_{(-)}} \bar{C}_{(+)} - \frac{\bar{Q}_v^0}{\omega_{(-)} e} \quad (5)$$

The number of cations and anions in the chemical formula of CaCl_2 is $v_{(+)} = 1$ and $v_{(-)} = 2$. Moreover, the charge of cation and anion are $\omega_{(+)} = 2$ and $\omega_{(-)} = 1$ respectively.

After obtaining $\bar{C}_{(-)}$ by solving Equation (4), $\bar{C}_{(-)}$ can be obtained from Equation (5).

On the other hand, in the intact-anion method, it is assumed that the anion concentration in the pore space is equal to the anion concentration in the reservoir, and the excess cation concentration balances the negative charge on the clay mineral surface in the pore space, i.e., we have (Revil, 2017):

$$\bar{C}_{(-)} = C_{(-)} = C_f \quad (6)$$

$$\bar{C}_{(+)} = C_{(+)} + \frac{\bar{Q}_v^0}{e} = C_f(1 + 2\theta) \quad (7)$$

The generalized form of the intact-anion method for a salt having $v_{(+)}$ cations with charge $\omega_{(+)}$ and $v_{(-)}$ anions with charge $\omega_{(-)}$ will be:

$$\bar{C}_{(-)} = C_{(-)} = v_{(-)}C_f \quad (8)$$

$$\bar{C}_{(+)} = C_{(+)} + \frac{\bar{Q}_v^0}{\omega_{(+)}e} = C_f(v_{(+)} + \frac{2}{\omega_{(+)}}\theta) \quad (9)$$

In the third method, namely the “intact method”, it is assumed that the concentration of ions in the shale after reaching equilibrium is the same as their concentration in the exterior solution.

2.1. Membrane efficiency

Revil et al. (2011) has derived the following equation for membrane efficiency based on the method for estimating the ionic concentration:

$$\text{Donnan method} \quad \varepsilon = 1 + \hat{\theta} \frac{\beta_{(+)}(\sqrt{\theta^2 + 1} + \theta) + \beta_{(+)}^s \Psi - \beta_{(-)}(\sqrt{\theta^2 + 1} - \theta)}{\beta_{(+)}(\sqrt{\theta^2 + 1} + \theta) + \beta_{(+)}^s \Psi + \beta_{(-)}(\sqrt{\theta^2 + 1} - \theta)} - \sqrt{\theta^2 + 1} \quad (10)$$

$$\text{Intact-anion method} \quad \varepsilon = \frac{\theta}{\theta + 1} + \frac{\hat{\theta}}{\theta + 1} \frac{\beta_{(+)}(2\theta + 1) + \beta_{(+)}^s \Psi - \beta_{(-)}}{\beta_{(+)}(2\theta + 1) + \beta_{(+)}^s \Psi + \beta_{(-)}} \quad (11)$$

where $\hat{\theta}$ is the dimensionless number of charge density dragged by pore water flow ($0 \leq \frac{\hat{\theta}}{\theta} = v \leq 1$), and v indicates a calibration parameter (Revil et al., 2011)). For a multivalent salt having $v_{(+)}$ cations with charge $\omega_{(+)}$ and $v_{(-)}$ anions with charge $\omega_{(-)}$, we derived a modified formula as:

$$\text{Donnan method} \quad \varepsilon = 1 + \hat{\theta} \frac{\omega_{(+)}\beta_{(+)}\bar{C}_{(+)} + \omega_{(+)}\beta_{(+)}^s \Psi C_f - \omega_{(-)}\beta_{(-)}\bar{C}_{(-)}}{\omega_{(+)}\beta_{(+)}\bar{C}_{(+)} + \omega_{(+)}\beta_{(+)}^s \Psi C_f + \omega_{(-)}\beta_{(-)}\bar{C}_{(-)}} - \frac{\frac{\bar{C}_{(+)}}{v_{(+)}} + \frac{\bar{C}_{(-)}}{v_{(-)}}}{2C_f} \quad (12)$$

$$\text{Intact-anion method} \quad \varepsilon = \frac{\theta}{\theta + 1} + \frac{\hat{\theta}}{\theta + 1} \frac{\omega_{(+)}\beta_{(+)}\bar{C}_{(+)} + \omega_{(+)}\beta_{(+)}^s \Psi C_f - \omega_{(-)}\beta_{(-)}\bar{C}_{(-)}}{\omega_{(+)}\beta_{(+)}\bar{C}_{(+)} + \omega_{(+)}\beta_{(+)}^s \Psi C_f + \omega_{(-)}\beta_{(-)}\bar{C}_{(-)}} \quad (13)$$

2.2. Ion selectivity

The electrochemical potential is measured by the setup shown in Figure 2c. This measured value is between a maximum (Nernst potential) and a minimum (liquid junction potential). The former (Equation (14)) is for the case where shale acts as a complete ion-selective membrane where anions are entirely excluded from entering into the shale, while the latter (Equation (15)) is for the case where there is no shale between the two reservoirs (Albazali, 2005). Since the extended Revil model considers the fluid as ideal, so $\gamma_1 = \gamma_2 = 1$.

$$V_{nr}\{mV\} = 1000 \frac{R T_0}{F} \ln \left(\frac{\gamma_2 C_f^2}{\gamma_1 C_f^1} \right) \quad (14)$$

$$V_{LJ} = (t_{(+)} - t_{(-)})V_{nr} \quad (15)$$

where $t_{(+)}$ and $t_{(-)}$ are the transport numbers of cation and anion calculated by (Revil, 2011):

$$t_{(\pm)} = \frac{\beta_{(\pm)}}{\beta_{(+)} + \beta_{(-)}} \quad (16)$$

We derived the following equation, which appears similar to Equation (15), to estimate the electrochemical potential across shale:

$$\Delta\psi\{mV\} = 1000 \frac{R T_0}{F} (T_{(+)} - T_{(-)}) \ln \left(\frac{C_f^2}{C_f^1} \right) = (T_{(+)} - T_{(-)})V_{nr} \quad (17)$$

where $T_{(+)}$ and $T_{(-)}$ are macroscopic Hittorf numbers of cations and anions, respectively, and we have (Revil, 2011):

$$T_{(+)} + T_{(-)} = 1 \quad (18)$$

The macroscopic Hittorf number of cations is calculated by the following equations (Revil, 2017):

$$\text{Donnan method} \quad T_{(+)} = \frac{\beta_{(+)}(\sqrt{\theta^2 + 1} + \theta) + \beta_{(+)}^s \Psi}{\beta_{(+)}(\sqrt{\theta^2 + 1} + \theta) + \beta_{(+)}^s \Psi + \beta_{(-)}(\sqrt{\theta^2 + 1} - \theta)} \quad (19)$$

$$\text{Intact-anion method} \quad T_{(+)} = \frac{\beta_{(+)}(2\theta + 1) + \beta_{(+)}^s \Psi}{\beta_{(+)}(2\theta + 1) + \beta_{(+)}^s \Psi + \beta_{(-)}} \quad (20)$$

where the dimensionless Dukhin number is defined as (Revil, 2011):

$$\Psi = \frac{2\Pi_{-1}\Gamma_{(+)}}{C_f} \quad (21)$$

where Π_{-1} is the raw moment of order (-1) of the capillary radius function. Since we assumed the capillary radius to be constant, it is found that $\Pi_{-1} = \frac{1}{R}$. The surface density of positively charged sites on the mineral surface $\Gamma_{(+)}$ is estimated from shale properties (Revil et al., 2011).

The ion selectivity is defined by (Albazali 2005):

$$IS = \frac{\Delta\psi - V_{LJ}}{V_{nr} - V_{LJ}} \quad (22)$$

By using Equations (15), (17), and (22), we derived:

$$IS = \frac{\Delta\psi - V_{LJ}}{V_{nr} - V_{LJ}} = \frac{(T_{(+)} - T_{(-)})V_{nr} - (t_{(+)} - t_{(-)})V_{nr}}{V_{nr} - (t_{(+)} - t_{(-)})V_{nr}} \rightarrow IS = \frac{T_{(+)} - t_{(+)}}{1 - t_{(+)}} \quad (23)$$

Again, for a multivalent salt having $v_{(+)}$ cations with charge $\omega_{(+)}$ and $v_{(-)}$ anions with charge $\omega_{(-)}$, we derived the following formula for $T_{(+)}$:

Donnan method or intact-anion method

$$T_{(+)} = \frac{\omega_{(+)}\beta_{(+)}\bar{C}_{(+)} + \omega_{(+)}\beta_{(+)}^s\Psi C_f}{\omega_{(+)}\beta_{(+)}\bar{C}_{(+)} + \omega_{(+)}\beta_{(+)}^s\Psi C_f + \omega_{(-)}\beta_{(-)}\bar{C}_{(-)}} \quad (24)$$

2.3. Comparison of experimental results with numerical data

The coefficient of determination (R^2), which is a measure of the correspondence of two data sets, is defined as follows. Denoting the observed data by Y_i and the fitted data by y_i , one may have:

$$\bar{Y} = \frac{1}{n} \sum_{i=1}^n Y_i \quad (25)$$

$$SS_{reg} = \sum_i (y_i - \bar{Y})^2, SS_{tot} = \sum_i (Y_i - \bar{Y})^2, SS_{res} = \sum_i (y_i - Y_i)^2 = \sum_i e_i^2 \quad (26)$$

$$R^2 \equiv 1 - \frac{SS_{res}}{SS_{tot}} \quad (27)$$

2.4. An analytical proof for Albazali's conjecture

Albazali (2005) and Lomba et al. (2000) guessed that there should be a direct relation between membrane efficiency and ion selectivity. We present analytical proof for this conjecture based on the extended Revil model outlined in this paper. Based on the simplified intact-anion method, which assumes that cation and anion mobility are the same $\beta_{(+)} = \beta_{(-)}$, one may obtain (Revil, 2011):

$$ME = \frac{\theta}{\theta + 1} \quad (28)$$

Using Equation (23), one may obtain:

$$\beta_{(+)} = \beta_{(-)} \rightarrow t_{(+)} = \frac{\beta_{(+)}}{\beta_{(+)} + \beta_{(-)}} = 0.5 \rightarrow IS = \frac{T_{(+)} - t_{(+)}}{1 - t_{(+)}} \approx \frac{T_{(+)} - 0.5}{1 - 0.5} = 2T_{(+)} - 1 \quad (29)$$

From Equation (20), by neglecting the term $\beta_{(+)}^s\Psi$, we obtain:

$$T_{(+)} \approx \frac{1 + 2\theta}{2 + 2\theta} \quad (30)$$

$$IS \approx 2 \times \frac{1 + 2\theta}{2 + 2\theta} - 1 = \frac{\theta}{\theta + 1} = ME \rightarrow IS \cong ME \quad (31)$$

However, the condition for the above equality, i.e., $\beta_{(+)} = \beta_{(-)}$, is often violated.

3. Experimental data

The membrane efficiency data in this study is from Albazali (2005), Manaka et al. (2018), Dominijanni et al. (2013), (2017a), and (2017b) (the latter containing two sets of data), Malusis et al. (2014), and Danyarov (2014).

The data set of Albazali (2005) is associated with four shale samples (C1, C2, Pierre shale, and Arco China) and four salts (NaCl, KCl, CaCl₂, and KHCO₂) at two salt concentrations, that is, at two water activities of $a_w = 0.85$ and 0.93 . The petrophysical properties are given in Table 1a.

A pressure transmission test measures membrane efficiency (ME). In this test, shale samples are put under hydraulic and osmotic gradients. The pressure drop between the two faces of the shale is measured.

Figure 2a shows a typical ME setup, and the pressure variation during the test is shown in Figure 2b. In the steady-state conditions, the value of upstream pressure minus downstream pressure is ΔP . This difference is due to the osmotic backflow caused by the higher water activity of the downstream pore fluid than that of the upstream fluid. The membrane efficiency is estimated by Equation (32) (Revil, 2017).

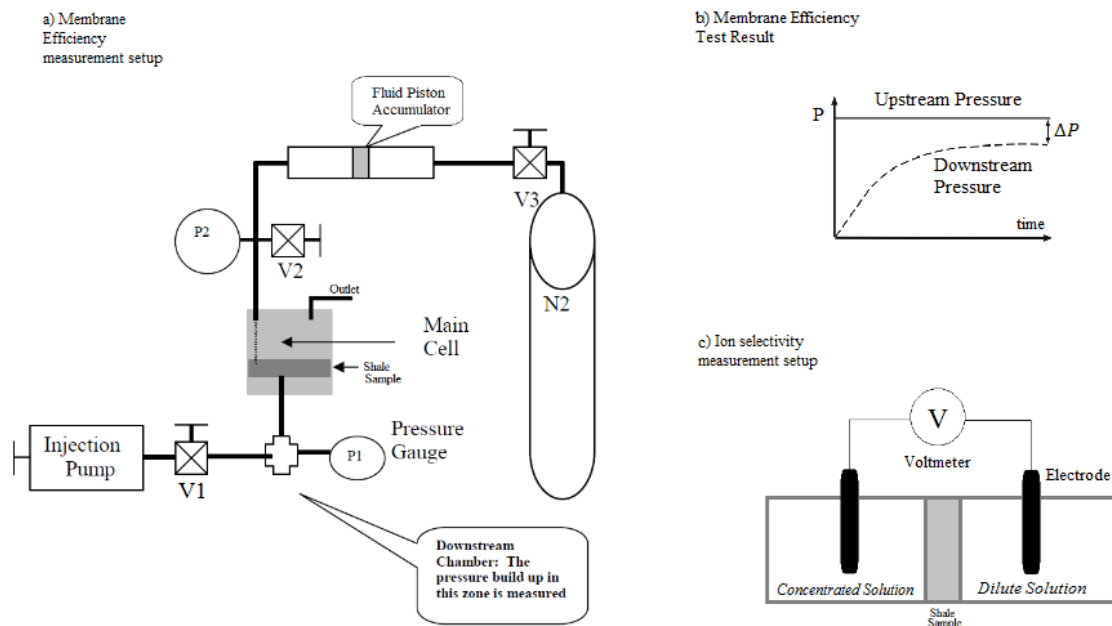


Figure 2

a) Membrane efficiency measurement setup, b) membrane efficiency test result, and c) ion selectivity measurement setup (Albazali, 2005).

$$ME = \frac{\Delta P}{\Delta \pi} \quad (32)$$

where ΔP is the actual pressure, and $\Delta\pi$ indicates the theoretical ideal osmotic pressure.

IS data used in this study are from Albazali (2005). The IS test is performed by placing the shale between two compartments having different salt concentrations (Figure 2c). In this way, an electrical potential is established, measured by a voltmeter. Ion selectivity is estimated by placing the measured potential in Equation (22). A summary of all data sets and the range of values of the main parameters are presented in Table 1b.

Table 1

a) Petrophysical data of Albazali 2005 and b) the summary of all the data sets used in this study.

a)

Shale	C1	C2	Pierre	Arco China
a_w , initial	0.98	0.94	0.98	0.85
CEC (meq/100gr)	21.0	23.0	10.5	24.5
Porosity	0.31	0.13	0.28	0.21

b)

Source	Albazali (2005)	Manaka et al. (2018)	Dominija nni et al. (2013)	Dominija nni et al. (2017a)	Dominija nni et al. (2017b/1)	Dominija nni et al. (2017b/2)	Malusis et al. (2014)	Daniyarov (2014)
Number of points	28	20	5	3	6	8	20	5
Rock type	Four natural shale samples	Mudstone	Bentonite	Sodium bentonite	Bentonite	Bentonite	GCL [†]	DPH-GCL [‡]
Porosity range	0.13–0.31	0.29–0.32	0.81	0.91	0.76–0.81	0.67–0.81	0.675–0.8	0.53–0.64
CEC range (meq/100gr)	10–25	21.5–33	105	105	105	48,105	48	52
C_f range	0.6–4 M	0.01–1 M	0–0.11 M	0.6–51 mM	5–86 mM	0–0.11 M	0.3–34 mM	0.4–148 mM
Salt types	NaCl, KCl, CaCl ₂ , KHCO ₂	NaCl, KCl, KHCO ₃	NaCl	NaCl	NaCl	NaCl, KCl	KCl	KCl

4. Simulation

We developed MATLAB codes to simulate the ionic concentrations of the pore space and estimate the membrane efficiency and ion selectivity based on the model outlined in the previous section.

[†] Geosynthetic clay liner

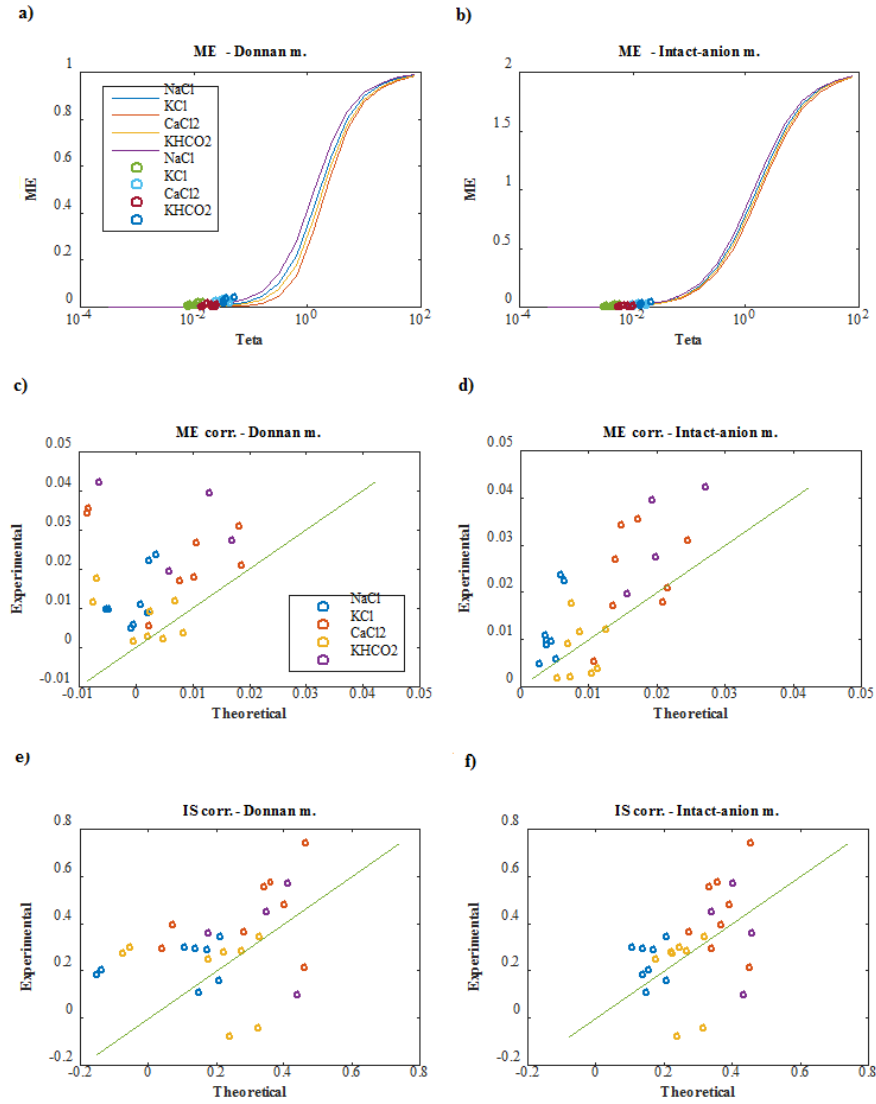
[‡] Dense Prehydrated GCL

5. Results and discussion

5.1. Membrane efficiency and ion selectivity

Transport parameters refer to membrane efficiency (ME) and ion selectivity (IS) parameters. Based on Equations (10)–(13) and (23), these parameters depend on the partition coefficient f_Q and on transport properties such as bulk and surface ion mobilities (i.e., $\beta_{(\pm)}$ and $\beta_{(+)}^S$) and the charge density dragged by pore fluid flow (i.e., ν). Here, the transport parameters, i.e., ME and IS, are considered in the steady-state conditions.

First, ME and IS data reported by Albazali (2005) have been obtained by both the intact-anion and Donnan methods, and the results have been compared with experimental data. The calibration parameters, i.e., f_Q , $\beta_{(+)}^S$, and ν , were manually adjusted to find some optimal values. As can be seen in Figure 3a, an acceptable correspondence is seen between ME data and typical ME curves obtained based on the model. However, because of small ME values in that zone, i.e., at low Θ and high concentrations, after magnification (Figure 3c), a significant discrepancy is revealed between the experimental data and the calculated values, demonstrating that the model should be investigated and modified for high concentrations, i.e., $C_f > 0.5$ M.

**Figure 3**

Prediction of ME and IS (Albazali's data (b, d), and f)) by the intact-anion method with the optimal parameters of $f_Q = 0.984$, $\nu = 1$, $\beta_{(+)}^S = 1$; (a, c, and e) by the Donnan method with optimal parameters of $f_Q = 0.95$, $\nu = 1$, $\beta_{(+)}^S = 1$.

However, using a case by case optimization via calibrating three parameters, namely f_Q , $\beta_{(+)}^S$, and ν , approximately a complete agreement between the model and the experimental data was obtained. It is observed that, in contrast to the Donnan method, ME values obtained by the intact-anion method are all positive, which is in a better consistency with the experimental values. The values of f_Q , $\beta_{(+)}^S$, and ν are close to 1.0. $\beta_{(+)}^S = 1$ indicates that the value of cation mobility in the Stern layer is equal to cation mobility in the free fluid. However, Revil et al. (2011) stated that the ion mobility in the Stern layer is naturally lower than the ion mobility in the free fluid.

For case by case calibration, the amount of ν is around 0.7 on average, implying that in the optimal conditions, about 0.7 of charge in the diffuse layer is considered to be dragged by the pore fluid flow, agreeing with the work of Revil (2017) stating that $\nu < 1$.

The ME values of CaCl_2 salt at two concentrations and four rock types, obtained by multivalent Equations (26) and (27) and monovalent Equations (24) and (25) are plotted versus the experimental ME values by Albazali 2005 to indicate the effectivity of the multivalent formulation developed in this study (Figure 4a and b). The multivalent formulation appears reasonable, while the monovalent formulation for multivalent salts is very inconsistent for both the intact-anion and Donnan methods.

In the following, the transport model is evaluated versus membrane efficiency data reported by Dominijanni et al. (2013) and (2017), Malusis et al. (2014), Danyarov (2014), and Manaka et al. (2018), along with two data sets presented in the previous section (Albazali, 2005). The results showed that the model has its best predictions for bentonites and is unsuccessful for natural shale.

In Figure 4c–f, various researchers' data sets of membrane efficiency have been compared with the model output. In both the intact-anion and Donnan methods, after manually adjusting the three parameters (f_Q , $\beta_{(+)}^S$, and ν), an excellent correlativity with the empirical data has been obtained. In the intact-anion curve (Figure 4c), the intact-anion method, in contrast to the Donnan method, shows an unexpected result, as for Θ values somewhat higher than 1.0; the amount of ME will be higher than 1.0, and at higher Θ values, it even approaches 2.0. However, in the range of experimental data, the modeled ME values are lower than 1.0, and ME values higher than 1.0 are assumed nonphysical.

The value of the partition coefficient f_Q was found close to 1.0, which is consistent with the results presented by Revil et al. (2004). This high value means that most counter-ions in the pore space accumulate in the Stern layer and adjacent to the mineral-fluid interface.

By adjusting the three parameters (f_Q , $\beta_{(+)}^S$, and ν), the values of R^2 for all the data sets, except for Albazali (2005) and Manaka et al. (2018), were higher than 0.9 for both the intact-anion and Donnan methods as presented in Table 2.

Table 2
Coefficient of determination (R^2) between the calculated values and measured data for different methods.

Charge distribution model	Data set	R^2 (Coefficient of determination) ion, water
Donnan method	Manaka (2018)	0.566855
	Dominijanni (2013)	0.926732
	Dominijanni (2017a)	0.922498
	Dominijanni (2017a)	0.916831
	Dominijanni (2017a)	0.914924
	Malusis (2014a)	0.914822
	Malusis (2014b)	0.909763
	Manaka (2018)	0.621352
	Dominijanni (2013)	0.916029
	Dominijanni (2017a)	0.915546
Intact-anion method	Dominijanni (2017a)	0.914503
	Dominijanni (2017a)	0.928502
	Malusis (2014a)	0.923417
	Malusis (2014b)	0.910594
	Manaka (2018)	0.621352
Donnan method	All ME data	0.93422

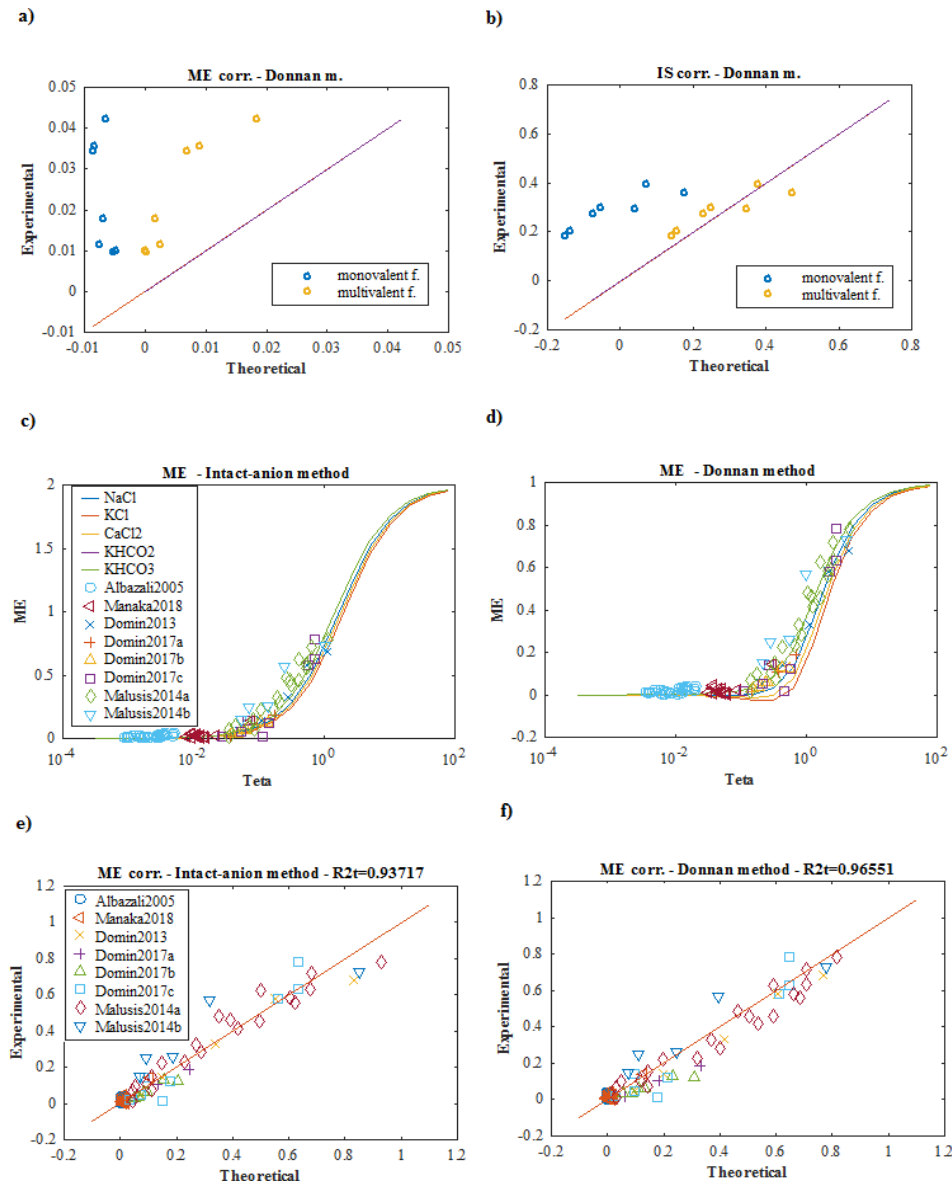
Charge distribution model	Data set	R^2 (Coefficient of determination) ion, water
Intact-anion method	All ME data	0.94068

An important observation associated with the results shown in Figure 3c–f is that the theory, in most cases, appropriately predicts the trend of change in the experimental values of ME and IS with change in the salinity, when the rock type and salt type are the same.

Figure 3c–f shows a systematic clustering of data points. For example, in most cases, seven points related to each salt can be divided into four sets (three pairs and one single point) corresponding to four rock types. Points of each pair, which have the same rock and salt types but different salinities, are somewhat close together and have a trend similar to the line $x = y$ and a similar offset from that line.

Moreover, in Figure 4c–f, different data sets have different offsets from the $x = y$ line because we have used a single set of calibration parameters for all data sets while those parameters are physically dependent on experimental attributes such as rock type. Nonetheless, the difference in the offsets is not significant.

As another confirmation for the proposed model, we present a water and ion flow simulation through the shale, matched with experimental data from Shoormasti and Tabatabaeinezhad (2021). The experimental data are from Manaka et al. (2018), and the experimental setup is shown in Figure 5, where the subscript *df* denotes drilling fluid properties. It comprises a shale slice (1 cm thick) placed between two closed chambers with initially different concentrations. The pressure of the left chamber is constant (p_{df}), and the pressure of the right chamber and the concentration in both chambers (C_0 and $C_{df} < C_0$) are measured during the time. As a result of osmosis, the pressure of the right chamber suddenly increases, and then, as a result of the diffusion of ions, it gradually declines (Figure 6b). Columns of Table 3 list the measured properties, except for the first four columns used as calibration parameters of the model. As Figure 6 shows, a successful matching could be obtained by tuning the calibration parameters.

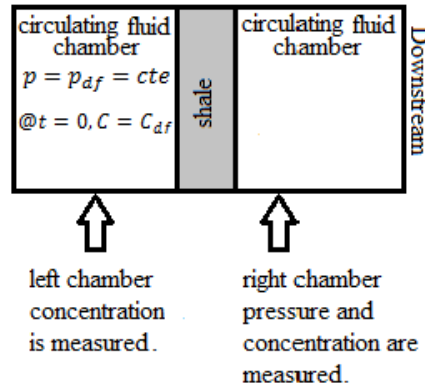
**Figure 4**

(a and b) Comparing monovalent Equations (24) and (25) with multivalent Equations (26) and (27) for predicting the membrane efficiency of CaCl₂ solutions. The experimental data are from Albazali (2005). It is observed that multivalent formulation is effective. The calibration parameters were $f_Q = 0.977$, $\nu = 1$, and $\beta_{(+)}^S = 1$. (c–f) the prediction of all the ME data sets: (c and e) by the intact-anion method with optimal calibration parameters of $f_Q = 0.995$, $\nu = 1$, and $\beta_{(+)}^S = 0.1$; (d and f) by the Donnan method with optimal calibration parameters of $f_Q = 0.98$, $\nu = 1$, and $\beta_{(+)}^S = 0.1$.

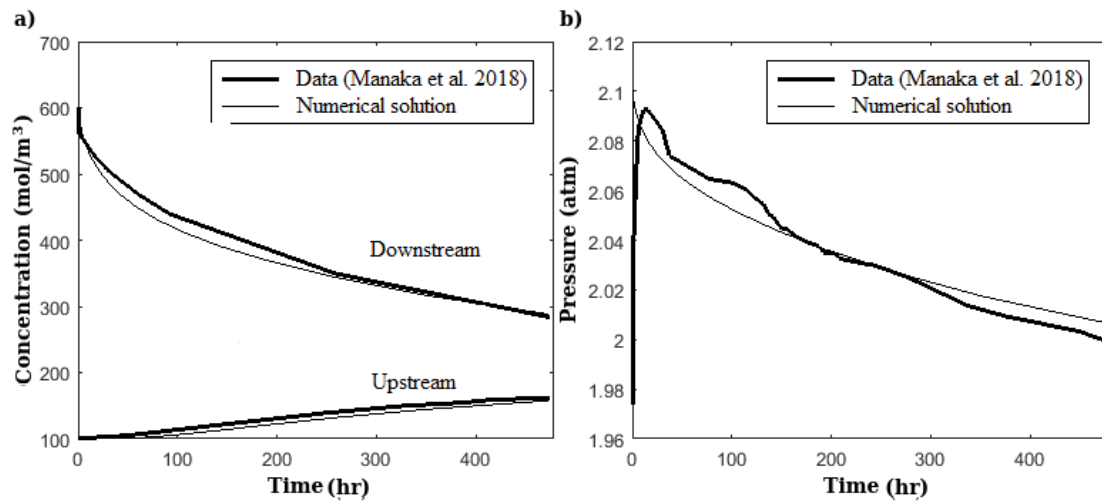
Table 3

Rock, solution, and experiment properties used in the simulation. The first four columns are considered the calibration variables. The following columns are specified by the experimental results of Manaka et al. (2018). The solution is assumed to follow the intact-anion model.

f_Q	ν	$\beta_{(+)}^S$	M	ϕ	CEC	ρ_g	k	C_0	C_{df}	L	Salt	Setup
					meq/gr	kg/m ³	m ²	mol/m ³	mol/m ³	cm		
0.997	0.7	0	2.8	0.32	0.29	2330	5×10^{-19}	100	600	1	KCl	Figure 5

**Figure 5**

The chemo-osmotic test setup used by Takeda et al. (2014) and Manaka et al. (2018) (Shoormasti and Tabatabaeinezhad, 2021).

**Figure 6**

Matching the concentration and pressure simultaneously downstream for the experimental data from Manaka et al. (2018) (Shoormasti and Tabatabaeinezhad, 2021).

5.2. Sensitivity analysis

A simple single variable sensitivity analysis was performed to investigate the uncertainty of the model. Figures 7 and 8 present the sensitivity analysis results considering the results shown in Figure 4b and 4d as the base cases; x and y axes are reversed. Each time one of the rock textural properties (i.e., porosity, CEC, m , and k) were either increased or decreased by 10%, the effect on the model prediction for membrane efficiency was evaluated and plotted in Figure 7. The plots depicting the effects of change of m and k on ME are not shown because those effects are negligible. As can be seen, the effect of 10% change in the porosity is higher than a similar change in the CEC. Figure 7a and b reveal that the model can fit almost all the data considering a tolerance of 10% in the accuracy of porosity values. Increasing the porosity causes the plot to go downward, while increasing the CEC causes the plot to go upward.

Similarly, each time one of the calibration parameters (f_Q , $\beta_{(+)}^S$, and ν) are changed, and the effect on model prediction for membrane efficiency is evaluated and plotted in Figure 8. The plot for the effect of change of $\beta_{(+)}^S$ on ME is not shown because this effect is negligible.

For sensitivity analysis with respect to ν (Figure 8a and b), three values of 1.0, 0.9, and 0.81 were considered. In contrast to other analyses, the base case data are not shown in the graph by markers but are located in the upper end of the various segments. The Donnan method is sensitive to change in ν values, while the intact-anion method is not. Increasing the ν value causes the plot to go downward.

For sensitivity analysis with respect to f_Q , a positive or negative 0.5% change in f_Q values with respect to the base case was considered. It is seen that the Intact-anion method is sensitive to change in f_Q values while the Donnan method is not (Figure 8c and d). Increasing f_Q causes the plot to go downward.

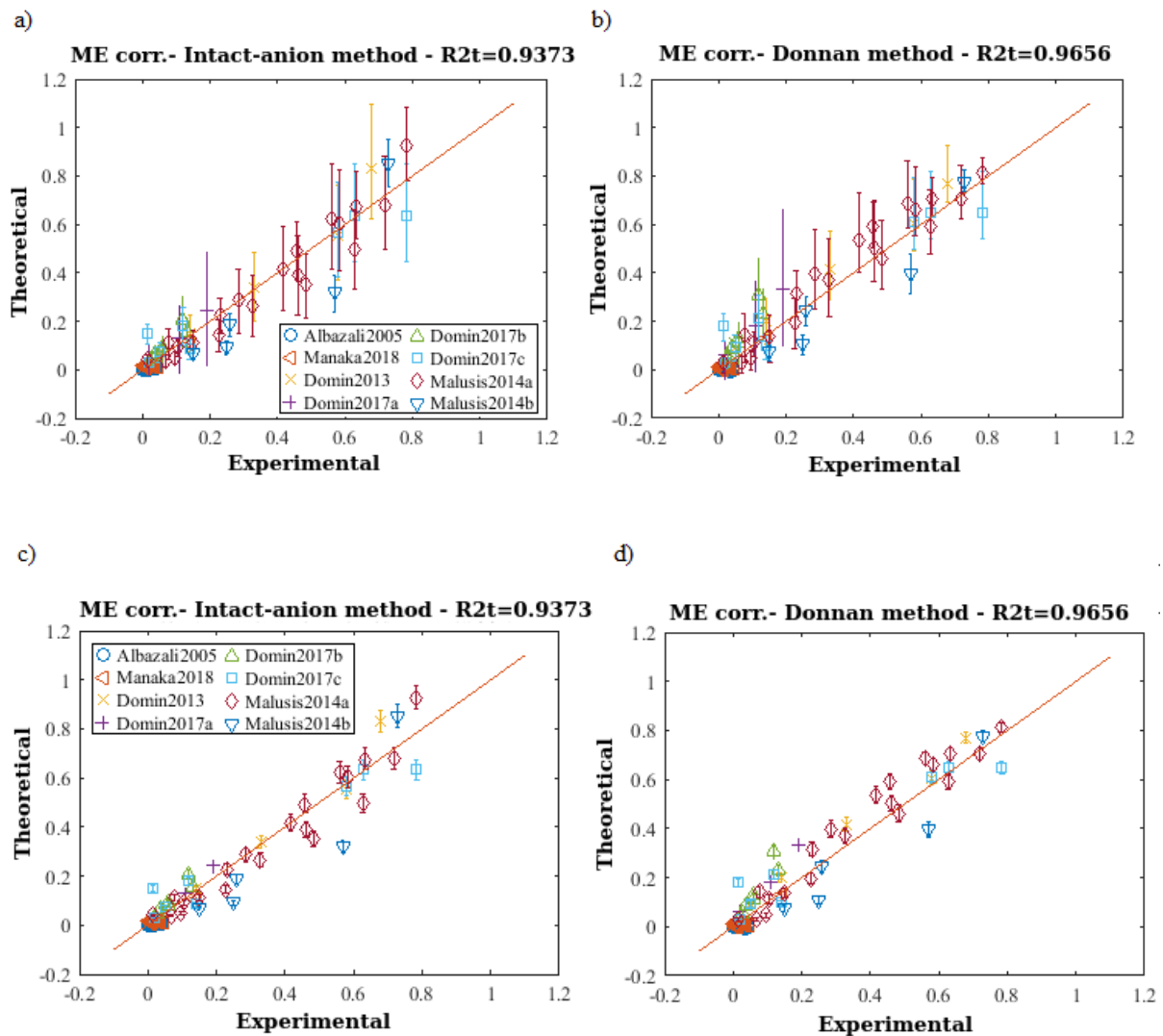
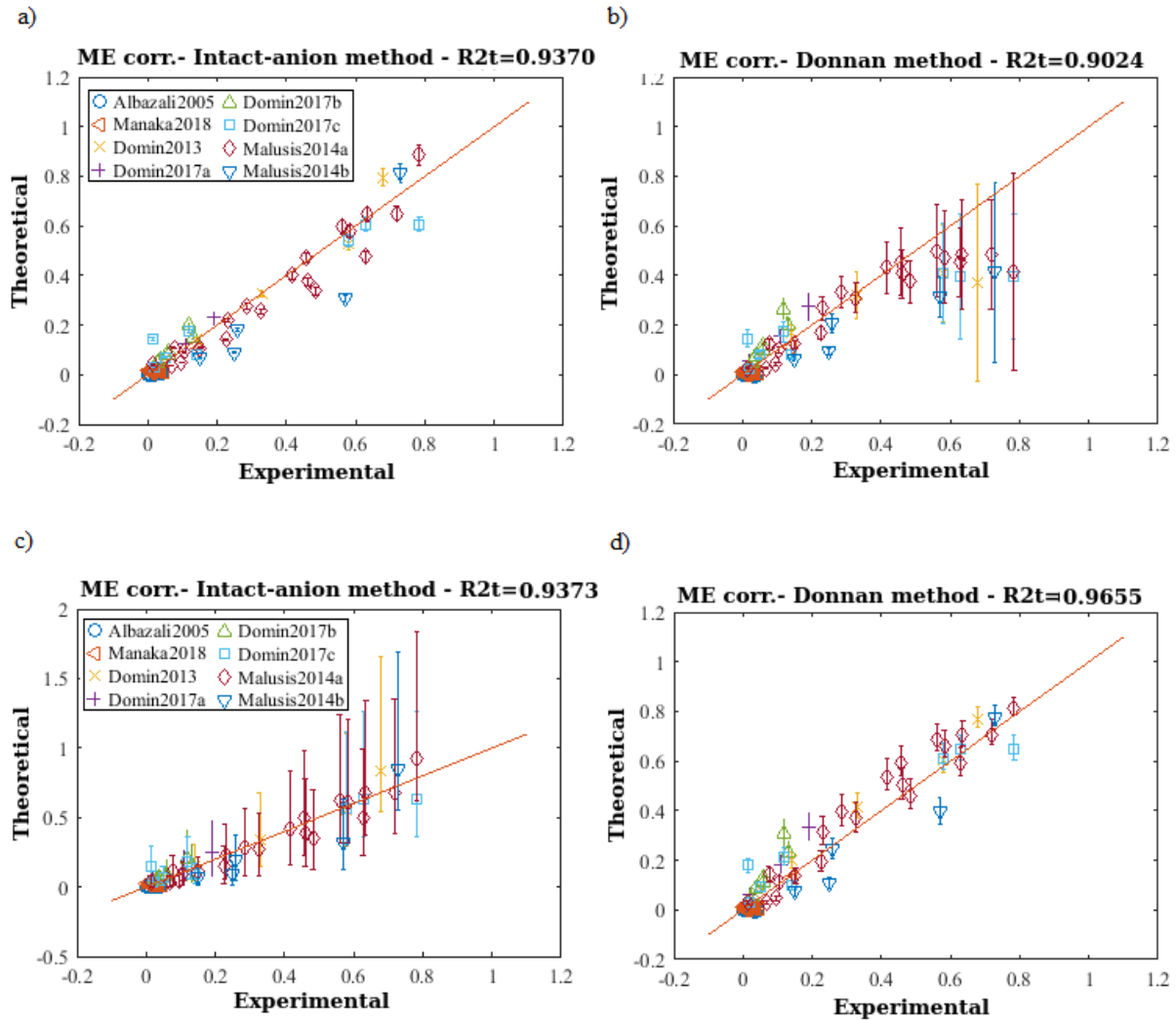


Figure 7

The results of the sensitivity analysis of model versus 10% change in (a and b) porosity and (c and d) CEC with respect to the base case (i.e., Figure 4e and f). The results show that porosity has a more significant effect on membrane efficiency than CEC. By assuming 10% tolerance in the measured porosity values, almost all data points can be fitted on the accurate prediction line $x = y$. x and y coordinates are reversed compared with Figure 4e and f.

**Figure 8**

The results of the sensitivity analysis of model versus change in the calibration parameters, namely (a and b) v and (c and d) f_Q with respect to the base case (i.e. Figure 4e and f). (a and b) Three values of v equal to 1.0, 0.9, and 0.81 were considered by assuming $\beta_{(+)}^S = 0.1$ and $f_Q = 0.995$ (for the intact-anion method) and $f_Q = 0.98$ (for the Donnan method). (c and d) a 5% change (positive or negative) in f_Q was applied with respect to the base case (i.e., Figure 4e and f) assuming the two other calibration parameters intact, i.e. $\beta_{(+)}^S = 0.1$ and $v = 1$. It is observed that changes in f_Q are effective in the intact-anion method, while the changes in v are effective in the Donnan method.

6. Conclusions

In the current study, the Revil model was extended for salts of multivalent ions and suggested as a valuable and novel tool for analyzing the empirical data of osmotic transport through shale. It is perceived that the model, notably the “intact-anion method”, predicts the data in the entire range of Θ values, especially for the higher Θ range, where the model has acceptable accuracy.

As a significant result of the current study, fitting all the experimental data sets (ME and IS) by calibrating three parameters (f_Q , $\beta_{(+)}^S$, and v) led to a high coefficient of determination ($R^2 > 0.9$) for the whole set of membrane efficiency data.

The novel mechanistic approach is at the intersection of thermodynamics and porous media modeling. The candidates for further research are anisotropy, pore size distribution, deformation, non-ideal solutions, and non-isothermal processes. More theoretical and experimental studies are needed to obtain better results at high concentrations and various shale types.

Nomenclature

CEC	Cation exchange capacity	C kg^{-1}
$C_{(\pm)}$	The concentration of cation and anion in the reservoir	mol m^{-3}
$\bar{C}_{(\pm)}$	The average concentration of cation and anion in the reservoir in porous shale	mol m^{-3}
C_f	Salt concentration in the reservoir	mol m^{-3}
e	Electron charge: $e = 1.6 \times 10^{-19}$	C
F	Faraday constant: $F = 96485$	s A mol^{-1}
f_Q	Fraction of extra cations of pore fluid in Stern layer	dimensionless
IS	Ion selectivity	dimensionless
ME	Membrane efficiency	dimensionless
N_{av}	Avogadro number: $N_{av} = 6.02 \times 10^{23}$	dimensionless
\bar{Q}_V	Volumetric charge density in the pore space	C m^{-3}
R	Gas constant: $R = 8.314$	$\text{J mol}^{-1}\text{K}^{-1}$
R	Capillary radius	m
$t_{(\pm)}$	Ionic transport numbers of cation and anion	dimensionless
$T_{(\pm)}$	Macroscopic Hittorf numbers of cation and anion	dimensionless
T_0	Temperature	K
V_{LJ}	Liquid junction potential between two electrolytes with different salt concentrations	mV
V_{nr}	Nernst potential	mV
$\beta_{(\pm)}$	Ionic mobility of cation and anion	$\text{m}^2\text{s}^{-1}\text{V}^{-1}$
$\beta_{(\pm)}^S$	Ionic mobility of cation and anion in Stern layer	$\text{m}^2\text{s}^{-1}\text{V}^{-1}$
$\Delta\psi$	Measured or modeled electric potential between two faces of shale placed between two electrolytes with different concentrations	mV
ϕ	Connected porosity	dimensionless
γ	The activity coefficient of salt solution	dimensionless
$\Gamma_{(+)}$	The surface density of cation-absorbing surface sites of shale	m^{-2}
$v_{(\pm)}$	Number of anions and cations in the chemical formula of the salt	dimensionless
$\rho_g \text{ or } f$	Grain or fluid density	kg m^{-3}
Θ	Dimensionless number of charge density of the diffuse layer	dimensionless
$\hat{\Theta}$	Dimensionless number of charge density dragged by pore water flow	dimensionless
Π_n	Raw moment of order n of the capillary radius distribution function $g(R)$	m^n
Ψ	Dukhin number	dimensionless

$\omega(\pm)$	Charge of anion and cation	dimensionless
---------------	----------------------------	---------------

References

- Albazali, T. M., Experimental Study of The Membrane Behavior of Shale during Interaction with Water Based and Oil-based Muds, Phd Thesis, University of Texas, Austin, 306 p., 2005.
- Basu, S., Sharma, M. M., An Improved Space-charge Model for Flow through Charged Microporous Membranes, *Journal of Membrane Science*, Vol. 124, p. 77-91, 1997.
- Chenevert, M. E., and Amanullah, M., Shale Preservation and Testing Techniques for Borehole-Stability Studies, SPE/IADC Drilling Conference, Society of Petroleum Engineers, 2001.
- Daniyarov, A. S., Relationship between Membrane Efficiency and Solute Diffusion Through A Dense, Prehydrated Geosynthetic Clay Liner, Master's Thesis, Bucknell University, 111 p., 2014.
- Dominijanni A., M. Manassero and Puma, S., Coupled Chemical-hydraulic-mechanical Behavior of Bentonites, *Geotechnique*, Vol. 63, No. 3, p. 191–205, 2013.
- Dominijanni, A., Musso, G., Cosentini, R. M., Guarena, N., Manassero, M., Laboratory Characterization of The Chemo-hydronechanical Behaviour of Chemically Sensitive Clays, *Rivista Italiana Di Geotecnica*, Vol. 51, No. 3, p. 22-47, 2017a.
- Dominijanni, A., Guarena, N., Manassero, M., Laboratory Assessment of The Semipermeable Properties of Natural Sodium Bentonite, *Canadian Geotechnical Journal*, Vol. 55, No. 11, p. 1611-1631, 2017b.
- Farrokhrouz M., Asef, M.R., *Shale Engineering: Mechanics and Mechanisms*, CRC Press, 2013.
- Gross R. J., Osterle, J. F., Membrane Transport Characteristics of Ultrafine Capillaries, *The Journal of Chemical Physics*, Vol. 49, No. 1, p.228-234, 1968.
- Kedem, O., And Katchalsky, A., Thermodynamics Analysis of The Permeability of Biological Membranes To Non-electrolytes, *Biochim, Biophys, Acta*, Vol.27, p. 229–246, 1958.
- Lomba, R. F. T., Chenevert, M. E., Sharma, M. M., The Ion Selective Behavior of Native Shale, *Journal of Petroleum Science and Engineering*, Vol. 25, No. 1-2, p. 9–23, 2000.
- Malusis, M. A., Kang, J. B., Shackelford, C. D., Restricted Salt Diffusion in A Geosynthetic Clay Liner, *Environmental Geotechnics*, Vol. 2, No. 2, p. 68-77, 2014.
- Malusis, M. A., Shackelford, C. D., and Olsen, H. W., Flow and Transport Through Clay Membrane Barriers, *Engineering Geology*, Vol. 70, No. 3-4, 235–248, 2003.
- Manaka, M., And Takeda, M., An Experimental Examination of The Effect of The Salt Type on The Chemoosmotic, Diffusive, and Hydraulic Parameters of Wakkanai Mudstones, *Journal of Hydrology*, Vol. 564 p. 1058–1073, 2018.
- Moslemizadeh, A., and Shadizadeh, S. R., Minimizing Water Invasion Into Kazhdumi Shale Using Nanoparticles, *Iranian Journal of Oil & Gas Science and Technology*, Vol. 4, No. 4, p. 15-32, 2015.
- Revil, A., Ionic Diffusivity, Electrical Conductivity, Membrane and Thermoelectric Potentials in Colloids and Granular Porous Media: A Unified Model, *Journal of Colloid and Interface Science*, Vol.,212, No.2, p.503-522, 1999.
- Revil, A., and Leroy, P., Constitutive Equations for Ionic Transport in Porous Shales, *Journal of Geophysics Research*, Vol. 109, No. B03208, 2004.

- Revil, A., Woodruff, W.F., Lu, N., Constitutive Equations for Coupled Flows in Clay Materials, *Water Resource Research*, Vol. 47, No. 5, 2011.
- Revil, A., Transport Properties Through Partially Saturated Charged Membranes and Geophysical Approaches, *Developments in Clay Science*, Vol. 6C, p. 357-398, 2015.
- Revil, A., Transport of Water and Ions in Partially Water-saturated Porous Media, Part 2. Filtration Effects, *Advanced Water Resource*, Vol. 103, p. 139-159, 2017.
- Revil, A., Ahmed A. S., Matthai, S., Transport of Water and Ions in Partially Water-saturated Porous Media, Part3. Electrical Conductivity, *Advances in Water Resources*, Elsevier, Vol. 121, p.97-111, 2018.
- Sen, P. N., Unified Model of Conductivity and Membrane Potential of Porous Media. *Physical Review B*, Vol.39, No.13, 9508p., 1989.
- Shoormasti, N. H., and Tabatabaeinezhad, A. A Novel Mechanistic Approach to Interpret Results of Chemo-osmotic Tests, in *E3S Web of Conferences*, EDP Sciences, Vol. 266, p. 01018, 2021.
- Spiegler, K. S., Yoest, R. L., & Wyllie, M. R. J., Electrical Potentials Across Porous Plugs and Membranes, Ion-Exchange Resin-solution Systems, *Discussions of The Faraday Society*, Vol.21, p.174-185, 1956.

Appendix A

First, we find equations for the electrochemical potential of multivalent ions corresponding to what is introduced in Revil et al. (2004) for monovalent ions. In a free fluid, the chemical potential of ions is defined by Equation (A1). Superscript R refers to a reference state (Revil et al., 2004).

The electrochemical potential of ions in the shale is given by Equation (A2). φ_0 denotes electrical potential in shale pore water, and overbar indicates properties in the pore water of shale.

$$\mu_{(\pm)}^0 = \mu_{(\pm)}^R + k_b T_0 \ln C_{(\pm)}^0 \quad (\text{A1})$$

$$\bar{\mu}_{(\pm)}^0 = \bar{\mu}_{(\pm)}^R + k_b T_0 \ln \bar{C}_{(\pm)}^0 \pm \omega_{(\pm)} e \bar{\varphi}_0 \quad (\text{A2})$$

k_b is Boltzmann constant ($k_b = 1.38 \times 10^{-23}$). As a result of thermodynamic equilibrium between brine outside shale and the pore water, one may obtain (Revil et al., 2004):

$$\mu_{(\pm)}^R = \bar{\mu}_{(\pm)}^R \quad (\text{A3})$$

$$\mu_{(\pm)}^0 = \bar{\mu}_{(\pm)}^0 \quad (\text{A4})$$

By dividing plus and minus versions of Equations (A1) and (A2) by $\omega_{(\pm)}$ and $\omega_{(\pm)}$ respectively and some manipulations, Equation (A5) is expressed by:

$$\bar{C}_{(+)} \frac{1}{\omega_{(+)}} \bar{C}_{(-)} \frac{1}{\omega_{(-)}} = C_{(+)} \frac{1}{\omega_{(+)}} C_{(-)} \frac{1}{\omega_{(-)}} \quad (\text{A5})$$

On the other hand, outside the shale pore space, in a free salt solution, we have:

$$C_{(\pm)} = v_{(\pm)} C_f \quad (\text{A6})$$

Further, by writing definition of \bar{Q}_v^0 as excess positive charge density in the pore space, we have:

$$\bar{Q}_v^0 = \bar{C}_{(+)} \omega_{(+)} e - \bar{C}_{(-)} \omega_{(-)} e \quad (\text{A7})$$

Equation (4) is obtained by rearranging:

$$\bar{C}_{(-)} = \frac{\omega_{(+)}}{\omega_{(-)}} \bar{C}_{(+)} - \frac{\bar{Q}_v^0}{\omega_{(-)} e} \quad (\text{A8})$$

Equation (5) is calculated using Equations (A5), (A6), and (A8):

$$\frac{\omega_{(+)}}{\omega_{(-)}} \bar{C}_{(+)}^{\frac{\omega_{(-)}}{\omega_{(+)}}+1} - \left(\frac{\bar{Q}_v^0}{\omega_{(-)} e} \right) \bar{C}_{(+)}^{\frac{\omega_{(-)}}{\omega_{(+)}}} - \left(v_{(-)} v_{(+)}^{\frac{\omega_{(-)}}{\omega_{(+)}}} C_f^{\frac{\omega_{(-)}}{\omega_{(+)}}+1} \right) = 0 \quad (\text{A9})$$